Conservative Scheme for a Compressible Nonhydrostatic Model with Moist Processes

MASAKI SATOH

Frontier Research System for Global Change/Saitama Institute of Technology, Saitama, Japan

(Manuscript received 28 March 2002, in final form 25 October 2002)

ABSTRACT

A conservative scheme for a compressible nonhydrostatic model including moist processes is formulated and is tested for experiments involving a squall line. The scheme is based on the flux form equations of total density, momentum, total energy, and the densities of water substance. The time-splitting scheme is used for the temporal scheme. In the small time step integration, the horizontal components of momentum are explicitly integrated, while the vertical components of momentum, density, and total energy are implicitly integrated. In particular, the flux form equation for the total energy is used to guarantee the conservation of the total energy. The internal energy is obtained by subtracting the kinetic energy and the potential energy from the total energy. This method is advantageous for the energy budget analysis. Only the warm rain cloud process is included for cloud physics. Using the squall-line experiments, the water budget and the energy budget are diagnosed and it is confirmed that the conservation of water and total energy is well satisfied.

As a quantitative improvement, more accurate formulas are used for the thermodynamics of the moist atmosphere by taking account of the effects of specific heats of the water substance and the temperature dependency of latent heat. These effects are generally neglected in most numerical models. If accurate moist thermodynamics are used, the total rain is reduced by more than 10% in comparison to the case when the simplified thermodynamics are used. The transportations of physical quantities due to rain are also appropriately introduced using a higher-order advection scheme. In the flux-form formulation, it is found that the change in energy due to the transportation of rain cannot be neglected in general, while that in momentum could be negligible.

1. Introduction

The understanding of the interactions between clouds and radiation is very important for the study of climate variability. Since the cloud feedback processes are ambiguously represented in the current global models (e.g., Tsusima and Manabe 2001), the importance of climate simulations with higher-resolution models that can directly resolve cloud motions is much appreciated. In a near future, it is thought possible to perform climate simulations with a long time integration using a high-resolution global model with horizontal resolution of less than 10 km. As the horizontal resolution of the models approaches a depth of the atmosphere of 10 km, the primitive equation models with the hydrostatic balance will be inappropriate for representation of the finest resolvable motions in the models. One should switch to using the nonhydrostatic equations for the global models instead of the hydrostatic primitive equations (Semazzi et al. 1995; Cullen et al. 1997; Qian et al. 1998; Smolarkiewicz et al. 2001; Yeh et al. 2002).

Cloud feedback processes are also studied by an another approach by using the regional nonhydrostatic models. Nowadays, the regional nonhydrostatic models are being used as cloud ensemble models (CEM) instead of cloud-resolving models (CRM). While CRMs are used for simulations of evolution of a single cloud, CEMs encompass simulations of interactions of number of cloud systems. As more and more numerical resources such as massive parallel computers become available, direct numerical calculations of moist convection in a wider domain are carried out using CEMs. For understanding cloud feedback processes, CEMs are used for calculations of statistical states of radiative–convective equilibrium by directly simulating moist convection for several tens of days in a region of more than several hundred kilometers (Nakajima and Matsuno 1988; Held et al. 1993; Tompkins and Craig 1998, 1999; Xu and Randall 1999; Tao et al. 1999; Tompkins 2001).

Most of the existing CEMs are developed, however, for a few days forecast on a regional scale and are not intended for climate simulations with long time integrations. In particular, numerical schemes of these regional models do not guarantee the conservation of physical quantities such as mass and energy, which are important for climate studies. Recently, conservative schemes of the nonhydrostatic models are proposed to overcome these shortcomings (Gallus and Rančić 1996; Klemp et al. 2000; Xue et al. 2000; Satoh 2002).

Corresponding author address: Dr. Masaki Satoh, Saitama Institute of Technology, 1690 Fusaiji, Okabe, Oosato, Saitama 369-0293, Japan.
E-mail: satoh@sit.ac.jp

TABLE 1. Physical constants.

Parameter	Value
Molecular weight of dry air	$m_d = 28.964 \times 10^{-3}$ kg mol^{-1}
Molecular weight of water	$m_w = 18.015 \times 10^{-3}$ kg mol^{-1}
Universal gas constant	$R^* = 8.3143$ J mol^{-1} K
Gas constant of dry air	$R_d = R^*/m_d = 287.04$ J kg^{-1} K^{-1}
Gas constant of vapor	$R_v = R^*/m_v = 461.50$ J kg^{-1} K^{-1}
Specific heat of dry air at constant pressure	$C_{pd} = 1004.6$ J kg^{-1} K^{-1}
Specific heat of dry air at constant volume	$C_{vd} = C_{pd} - R_d = 717.56$ J kg^{-1} K^{-1}
Specific heat of vapor at constant pressure	$C_{pv} = 1850.0$ J kg^{-1} K^{-1}
Specific heat of vapor at constant volume	$C_{vv} = C_{pv} - R_v = 1389.0$ J kg^{-1} K^{-1}
Specific heat of liquid water	$C_l = 4218.0$ J kg^{-1} K^{-1}
Latent heat at 0°C	$L_0 = 2.5008 \times 10^6$ J kg^{-1}
Latent heat at 0 K	$L_{00} = L_0 + (C_{pv} - C_l)\, T_0 = 3.14762 \times 10^6$ J kg^{-1}
Saturation vapor pressure at 0°C	$p_0^* = 610.7$ Pa
Reference pressure	$p_0 = 1.0 \times 10^5$ Pa
Reference temperature	$T_0 = 273.15$ K

The conservative scheme developed by Satoh (2002) is based on the flux form equations of density, momentum, and internal energy. The proposed nonhydrostatic model uses the horizontally explicit and vertically implicit time integration scheme for sound and gravity waves and can be extended to employ the time-splitting technique. Satoh (2002) intended to develop the numerical scheme in order to use it as a dynamical core of a high-resolution nonhydrostatic global circulation model, which is now being developed using the icosahedral grid proposed by Tomita et al. (2001). In Satoh (2002), only the formulation for the dry atmosphere is presented. Several experiments of the dry dynamics were performed and showed that the domain-averaged mass and total energy are well conserved. It is clear, however, that physical processes such as cloud, radiation, and turbulence must be introduced with appropriate boundary conditions in order to use the proposed numerical scheme for climate studies. Among them, the introduction of moist processes is the first key step to use the model as the CRM or the CEM. Only after its validity is confirmed through calculations of moist circulations in a regional model, we can proceed to the next step of the model development, that is, the development of a global cloud ensemble model.

Very recently, the treatment of moist processes in the flux form equations is considered by Ooyama (1990, 2001). Using the density and the moist entropy as prognostic variables, Ooyama obtained the saturation condition of air parcels. Ooyama also formulated the transportations of mass, momentum, and energy associated with precipitation. Although the governing equations of Satoh (2002) have many similarities to the flux form equations of Ooyama, Satoh (2002) uses the internal energy instead of the entropy as a prognostic variable to guarantee the conservation of energy. Since Ooyama's formulation is based on entropy, we need some modifications to Ooyama (2001) if moist processes are introduced.

Our ultimate goal is to develop a global nonhydrostatic climate model that can more accurately simulate interactions between clouds and radiation. In this study, as one of the necessary steps toward the goal and as an extension of Satoh (2002), we describe a formulation of the conservative nonhydrostatic equations with moist processes. Although the ice phase processes are very important for the realistic representation of clouds, we only consider the warm rain process to concentrate on the formulation of numerical schemes. In section 2, first, we review the moist thermodynamics. In particular, we use an accurate expression of moist energy by taking account of the effects of specific heats of water substance and dependency of the latent heat on temperature. Following the descriptions of the governing equations and the energy budget in section 3, we formulate a numerical scheme that guarantees the conservation of the domain-averaged mass, momentum, and total energy in section 4. We perform a couple of numerical experiments with moist convection in section 5. Conclusions are given in section 6.

2. Moist thermodynamics

The thermodynamic expressions of the moist atmosphere are reviewed in this section. We assume that air parcels consist of dry air, vapor, and liquid water, and that liquid water is further divided into cloud water and rainwater. Cloud water is in phase equilibrium with vapor in the air and is airborne, while rainwater is precipitating. All the liquid water has the same temperature as that of the surrounding air. We do not consider ice phase throughout this study. The symbols of the constants are listed in Table 1.

a. Latent heat and saturation vapor pressure

In general, the relations between the latent heat L, the specific heat of vapor at constant pressure C_{pv}, the specific heat of liquid water C_l, and the saturation vapor pressure p^* are given by Kirchhoff's law and the Clausius–Clapeyron equation:

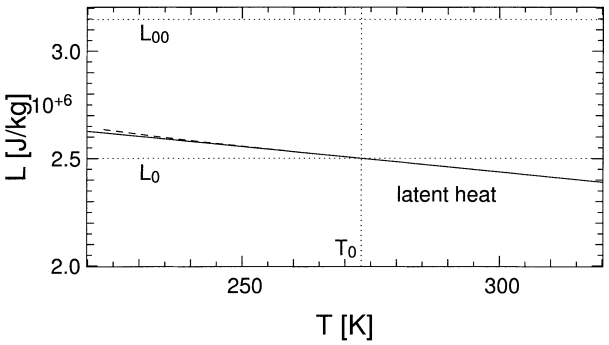

FIG. 1. Dependency of latent heat of vaporization on temperature (solid). Here, L_0 is the latent heat at $T_0 = 0°C$ and L_{00} is the latent heat at 0 K. The dashed line is based on List (1951).

$$\frac{dL}{dT} = C_{pv} - C_l, \qquad \frac{dp^*}{dT} = \frac{Lp^*}{R_v T^2}. \tag{1}$$

Neglecting temperature dependency of specific heats, we have consistent expressions for L and p^* with the above formulas as

$$\begin{aligned} L &= L_0 + (C_{pv} - C_l)(T - T_0) \\ &= L_{00} + (C_{pv} - C_l)T, \end{aligned} \tag{2}$$

$$p^*(T) = p_0^* \left(\frac{T}{T_0}\right)^{(C_{pv}-C_l)/R_v} \exp\left[\frac{L_{00}}{R_v}\left(\frac{1}{T_0} - \frac{1}{T}\right)\right], \tag{3}$$

where we have defined $L_{00} = L_0 + (C_{pv} - C_l)T_0$, which represents the latent heat at the temperature 0 K. It should be noted that L_{00} is quite different from L_0, which is the latent heat at 0°C as shown in Table 1. The dependency of the latent heat on temperature is displayed in Fig. 1. Compared with values between $-20°$ and 30°C from List (1951) the maximum errors of Eqs. (2) and (3) are 0.13% for the saturation vapor, and 0.046% for the latent heat. Thus, even if the specific heats are assumed to be constant, these expression give good approximations.

In some numerical models in meteorology, more accurate expressions of the saturation vapor pressure based on experimental formula such as Teten's formula or Goff–Gratch's equation are used. In such formulations, to keep the thermodynamic consistency, one needs to define a corresponding latent heat $L(T)$ from Eq. (1). In contrast, some models use the following simplified expressions:

$$L = L_0, \qquad p^*(T) = p_0^* \exp\left[\frac{L_0}{R_v}\left(\frac{1}{T_0} - \frac{1}{T}\right)\right]. \tag{4}$$

In this case, the use of a constant value L_0 may cause an quantitative error since it varies up to about 5% within the temperature range from $-20°$ to 30°C.

In Ooyama (1990), C_{pv} is assumed to be constant and a function $p^*(T)$ is externally specified to determine the temperature dependencies of $L(T)$ and $C_l(T)$. Although C_l is almost constant in fact, Ooyama (1990) introduced its dependency on temperature in order to integrally treat the latent heats and the saturation vapor pressures on water and ice. Since we do not consider the ice phase in this study, we do not follow Ooyama's approach and simply assume that the two specific heats are constant.

b. Thermodynamic expressions

We assume that all of the specific heats of dry air and water substance are constant irrespective of temperature (Table 1), and use the expressions of the latent heat [Eq. (2)] and the saturation vapor pressure [Eq. (3)]. We denote the mass concentration of dry air by q_d, that of vapor (or specific humidity) by q_v, and that of liquid water by q_l. We generally have $q_d + q_v + q_l = 1$. We also denote the total mass concentration of water substance by $q_w = q_v + q_l$. The mass concentration of liquid water is divided into that of cloud water, q_c, and that of rain, q_r: $q_l = q_c + q_r$. We denote the mass concentration of the sum of the airborne water substance by $q_m = q_v + q_c$. We neglect the volume of the liquid phase; this assumption is consistent with the Clausius–Clapeyron equation (1). The equation of state reads

$$p = \rho(q_d R_d + q_v R_v)T, \tag{5}$$

where ρ is total density and p is pressure.

The expressions of enthalpy h, internal energy e, and entropy s per unit mass are summarized as follows (e.g., Emanuel 1994). The subscripts d, v, and l are used to denote quantities of dry air, vapor, and liquid water per unit volume, respectively. In the case of a mixture of various phases, the expressions of energy depend on the origin of energy. We specify the origin of energy as the energy of the liquid water at 0 K: $h_l(T = 0\ \text{K}) = 0$. Thus, we generally have

$$h = q_d h_d + q_v h_v + q_l h_l, \tag{6}$$

$$e = h - \frac{p}{\rho} = q_d e_d + q_v e_v + q_l e_l, \quad \text{and} \tag{7}$$

$$s = q_d s_d + q_v s_v + q_l s_l, \tag{8}$$

where

$$h_d = C_{pd}T, \quad h_v = C_{pv}T + L_{00}, \quad h_l = C_l T \quad \text{and} \tag{9}$$

$$e_d = C_{vd}T, \quad e_v = C_{vv}T + L_{00}, \quad e_l = C_l T, \tag{10}$$

and

$$s_d = C_{pd} \ln\frac{T}{T_0} - R_d \ln\frac{p_d}{p_0} = C_{vd} \ln\frac{T}{T_0} - R_d \ln\frac{\rho_d}{\rho_0}, \tag{11}$$

$$s_v = C_{pv} \ln\frac{T}{T_0} - R_v \ln\frac{p_v}{p_0^*} + \frac{L_0}{T_0}$$

$$= C_{vv} \ln\frac{T}{T_0} - R_v \ln\frac{\rho_v}{\rho_0^*} + \frac{L_0}{T_0}, \quad \text{and} \tag{12}$$

$$s_l = C_l \ln\frac{T}{T_0}, \tag{13}$$

where $\rho_i = \rho q_i$ $(i = d, v, l)$, $p_i = \rho_i R_i T$ $(i = d, v)$, $p_0 = \rho_0 R_d T_0$, and $p_0^* = \rho_0^* R_v T_0$. We also have

$$h_v - h_l = L_{00} + (C_{pv} - C_l)T = L \quad \text{and} \tag{14}$$

$$e_v - e_l = L_{00} + (C_{vv} - C_l)T = L - R_v T. \tag{15}$$

Letting the entropy of vapor at saturation vapor pressure be s_v^*, we have

$$s_v^* - s_l = (C_{pv} - C_l)\ln\frac{T}{T_0} - R_v \ln\frac{p^*}{p_0^*} + \frac{L_0}{T_0} = \frac{L}{T}. \tag{16}$$

This equation is the definition of the latent heat and can be confirmed by substituting Eqs. (2) and (3).

c. Saturation condition

We assume air parcels are not supersaturated. On this assumption, the mass concentration of cloud water is diagnostically determined by the excess of water over the saturation vapor concentration. Hereafter, such a diagnostic calculation for the saturation condition is called the *adjustment process*. The values of vapor, cloud water, and temperature are redefined at the adjustment process. Denoting the mass concentration of the airborne water before the adjustment process as $q_m = q_v + q_c$, the vapor and the cloud water after the adjustment are diagnostically given by

$$q_v = \min(q_m, q_v^*(T)) \quad \text{and} \quad q_c = q_m - q_v, \tag{17}$$

where T is the temperature after the adjustment process and $q_v^*(T) = p^*(T)/(\rho R_v T)$ is the saturation specific humidity at temperature T. The density ρ does not change during the adjustment process.

We need to know whether air parcels are saturated or not if ρ, q_i $(i = v, c, r)$, and if e of air parcels are known. To determine the saturation condition, a method similar to the one proposed by Ooyama (1990, 2001) can be used. Ooyama compares the two temperatures for the case where all the water substance is contained as vapor and the case where vapor and liquid phases are in phase equilibrium under the condition that ρ, q_m, and the entropy s are given. We use the internal energy e instead of the entropy to estimate the temperatures for the two cases.

If all the cloud water is evaporated to vapor, the internal energy is expressed as

$$e = E_1(\rho, q_m, q_r, T) \equiv q_d e_d + q_m e_v + q_r e_l = [(1 - q_m - q_r)C_{vd} + q_m C_{vv} + q_r C_l]T + q_m L_{00}. \tag{18}$$

If the vapor and the cloud water are in phase equilibrium, the internal energy is given as

$$e = E_2(\rho, q_m, q_r, T) \equiv q_d e_d + q_v^* e_v + (q_c + q_r)e_l = [(1 - q_m - q_r)C_{vd} + (q_m + q_r)C_l]T + q_v^*(\rho, T)[L(T) - R_v T)]. \tag{19}$$

The above two equations are solved for temperature, T_1 and T_2, respectively. If supersaturation is prohibited, the realizable temperature is determined by

$$T = \max(T_1, T_2). \tag{20}$$

d. Change in internal energy due to latent heat release

The internal energy of the moist atmosphere e defined by Eq. (7) contains the contribution of the latent heat. This might cause a large error in the diagnostic estimation of temperature if the prediction of specific humidity is affected by numerical errors. In order to avoid these errors, the predictions of temperature and specific humidity are usually separated in most numerical models. In our formulation, although we do not choose temperature as a prognostic variable, we can formally separate the internal energy into the part proportional to temperature and the rest of it:

$$e = (q_d C_{vd} + q_v C_{vv} + q_l C_l)T + q_v L_{00} \equiv e_a + q_v L_{00} \quad \text{and} \tag{21}$$

$$e_a \equiv (q_d C_{vd} + q_v C_{vv} + q_l C_l)T. \tag{22}$$

Here, we may refer to e_a as the sensible heat part of the internal energy and $q_v L_{00}$ as the latent heat part. The total internal energy e can be called the moist internal energy. If phase change occurs under the condition that e and $q_m = q_v + q_c$ are constant, we have

$$\delta e_a = -\delta q_v L_{00} = \delta q_c L_{00}, \tag{23}$$

that is, e_a is increased by the latent heat release proportional to L_{00}, if a phase change from vapor to liquid water occurs. It should be noted that L_{00} is the latent heat at 0 K and is quite different from the latent heat at 0°C, L_0. Since the effects of specific heats of vapor and liquid water are already included in e_a, the net increase of e_a due to the change in q_v is proportional to $L - R_v T = (C_{vv} - C_l)T + L_{00}$.

In section 5, we will compare the numerical results using the above exact formula with those using a conventional formula of moist thermodynamics, in which $e = C_{vd}T + L_0 q_v$, $e_a = C_{vd}T$, and $L = L_0$ are used. In this case, change in internal energy due to the latent

heat release is given by $\delta e_a = \delta q_v L_0$. We will call the formula based on these conventional expressions the *simplified thermodynamics.*

3. Governing equations

Following Ooyama (2001), we use the flux form equations of the moist atmosphere including the ''warm rain'' process. The conservation equations of water substance (vapor, q_v; cloud water, q_c; and rainwater, q_r) are given by

$$\frac{\partial(\rho q_v)}{\partial t} + \nabla_H \cdot (\rho q_v \mathbf{v}_H) + \frac{\partial(\rho q_v w)}{\partial z} = -S_{\text{conv}} + S_{\text{evap}} + D_v, \quad (24)$$

$$\frac{\partial(\rho q_c)}{\partial t} + \nabla_H \cdot (\rho q_c \mathbf{v}_H) + \frac{\partial(\rho q_c w)}{\partial z} = S_{\text{conv}} - (S_{\text{auto}} + S_{\text{accr}}) + D_c, \quad \text{and} \quad (25)$$

$$\frac{\partial(\rho q_r)}{\partial t} + \nabla_H \cdot (\rho q_r \mathbf{v}_H) + \frac{\partial}{\partial z}[\rho q_r (w + w_r)] = (S_{\text{auto}} + S_{\text{accr}}) - S_{\text{evap}} + D_r, \quad (26)$$

where $\mathbf{v}_H = (u, v)$ is the horizontal components of velocity, w is the vertical velocity, and $\nabla_H = (\partial/\partial x, \partial/\partial y)$. The warm rain process is parameterized with the bulk method of Ooyama (2001) or Klemp and Williamson (1978), where w_r is the rainfall velocity (positive upward), S_{auto} is the generation rate of rain by autoconversion of cloud water into rain, S_{accr} is the generation rate of rain by accretion of cloud water, and S_{evap} is the evaporation rate of rainwater into vapor. Here, S_{conv} is the conversion rate from vapor to cloud water by condensation or evaporation, and is diagnostically calculated using the saturation condition described in section 2, and D_v, D_c, and D_r are diffusion terms. The corresponding conservation equation of dry air q_d is written as

$$\frac{\partial(\rho q_d)}{\partial t} + \nabla_H \cdot (\rho q_d \mathbf{v}_H) + \frac{\partial(\rho q_d w)}{\partial z} = D_d. \quad (27)$$

Summing up Eqs. (24)–(26) and (27), we obtain the conservation of mass, or the total mass density ρ, as

$$\frac{\partial \rho}{\partial t} + \nabla_H \cdot (\rho \mathbf{v}_H) + \frac{\partial}{\partial z}(\rho w + \rho q_r w_r) = 0, \quad (28)$$

where $D_d + D_v + D_c + D_r = 0$ is assumed.[1] The transport of mass due to rain $\rho q_r w_r$ enters into the vertical flux. We use the equation of total mass density (28) as one of the prognostic equations of the numerical model; in contrast, Ooyama (2001) and Klemp et al. (2000) use the equation of density of dry air [Eq. (27)].

Since the mass transport due to rain is introduced into the vertical flux of the equation of mass, the transformation formula from the flux form equation to the advective form equation has additional terms as derived by Ooyama (2001). If the flux form equation for a scalar quantity a is given as

$$\frac{\partial(\rho a)}{\partial t} + \nabla_H \cdot (\rho a \mathbf{v}_H) + \frac{\partial}{\partial z}[(\rho w + \rho q_r w_r) a] = S, \quad (29)$$

the corresponding advective form equation is written by using Eq. (28) as

$$\rho \frac{da}{dt} = -\rho q_r w_r \frac{\partial a}{\partial z} + S. \quad (30)$$

The equations of horizontal and vertical components of momentum are given as

$$\frac{\partial(\rho \mathbf{v}_H)}{\partial t} + \nabla_H \cdot (\rho \mathbf{v}_H \mathbf{v}_H) + \frac{\partial}{\partial z}(\rho \mathbf{v}_H w + \rho q_r \mathbf{v}_H w_r) = -\nabla_H p + \mathbf{F}_H \quad \text{and} \quad (31)$$

$$\frac{\partial(\rho w)}{\partial t} + \nabla_H \cdot (\rho w \mathbf{v}_H) + \frac{\partial}{\partial z}(\rho w w + \rho q_r w w_r) = -\frac{\partial p}{\partial z} - \rho g + F_z, \quad (32)$$

where $\mathbf{F}_H$ and F_z are the friction terms, and $\rho q_r \mathbf{v}_H w_r$ and $\rho q_r w w_r$ are the transports of momentum due to rain. To derive these equations, we use the assumptions as in Ooyama (2001); the horizontal components of the velocity of rainwater are the same as those of air, and the vertical component of velocity of rainwater is given by the terminal velocity w_r. We do not consider the Coriolis terms throughout this paper.

We use the equation of internal energy following Satoh (2002), which is different from that of Ooyama (1990, 2001), who uses the equation of entropy. We should note that there are two expressions of internal energy. The first is based on the moist internal energy e defined by Eq. (7). In this case, the equation of moist internal energy is given by

$$\frac{\partial(\rho e)}{\partial t} + \nabla_H \cdot (\rho h \mathbf{v}_H) + \frac{\partial}{\partial z}(\rho h w + \rho q_r e_r w_r) = -\mathbf{v} \cdot \nabla p - \rho q_r w_r g + Q'_H, \quad (33)$$

where $\rho q_r e_r w_r$ on the left-hand side is the transport of internal energy due to rain and $-\rho q_r w_r g$ on the right-hand side is the heat source due to the release of potential energy associated with precipitation. In general, $e_r = C_l T$. It should be noted that even if the specific heat of water is neglected using the simplified thermodynamics, the effect of energy change due to rain must be introduced; the appropriate choice in this case is $e_r = C_{vd} T$. The term Q'_H generally represents convergence of energy fluxes and contains the convergence of both sensible and latent heat fluxes. It should be noted that Q'_H does not contain the latent heat release.

As a second approach to the equation of internal en-

[1] Precisely, the constraint $D_d + D_v + D_c = 0$ holds since $\rho \mathbf{v}$ is the mass flux of the airborne components.

ergy, we can use the sensible heat part of the internal energy e_a defined by Eq. (22), which is proportional to temperature T. The departure of e_a from e is the latent heat part of the internal energy $q_v L_{00}$. We also define the sensible heat part of enthalpy by

$$h_a \equiv h - q_v L_{00} = (q_d C_{pd} + q_v C_{pv} + q_l C_l)T. \quad (34)$$

Thus, from Eqs. (33) and (24), we obtain

$$\frac{\partial}{\partial t}(\rho e_a) + \nabla_H \cdot (\rho h_a \mathbf{v}_H) + \frac{\partial}{\partial z}(\rho h_a w + \rho q_r e_r w_r) = -\mathbf{v} \cdot \nabla p - \rho q_r w_r g + L_{00}(S_{\text{conv}} - S_{\text{evap}}) + Q_H, \quad (35)$$

where $L_{00}(S_{\text{conv}} - S_{\text{evap}})$ is the latent heat release and $Q_H = Q'_H - L_{00} D_v$ is the diabatic heating.

As shown above, we need to consider the transports of momentum and energy due to rain in the flux form equations, in general. The computational cost for the transports due to rain might be high if an accurate transportation scheme is used. Thus, we are motivated to estimate these effects whether they can be negligible or not in order to save the computational cost. To simplify the argument, we consider a situation where rainwater is supplied to a dry atmosphere and estimate changes after all the supplied rainwater is fallen out. If the effect of the transport of energy due to rain is neglected, the internal energy in a control volume remains the same: $E \equiv \rho(q_d C_{vd} + q_r C_l)T = \rho' C_{vd} T'$, where $q_d = 1 - q_r$, and the primed quantities are the values after the rainwater is taken out. Using $\rho' \approx \rho(1 - q_r)$ and a typical rainwater content $q_r \approx 10^{-3}$ kg kg^{-1}, the change in temperature is estimated as

$$\Delta T = T' - T = \frac{q_r C_l}{(1 - q_r) C_{vd}} T \approx \frac{10^{-3} \times 4218}{717} \times 300 = 1.8 \text{ K}. \quad (36)$$

This error is very large and may enhance the development of moist convection. This means that we must not neglect the effect of the transport of energy due to rain in the flux form formalism. In the case where the simplified thermodynamics are used, since $E \equiv \rho C_{vd} T = \rho' C_{vd} T'$, the change in temperature is also estimated as

$$\Delta T = T' - T = \frac{q_r}{1 - q_r} T \approx 10^{-3} \times 300 = 0.3 \text{ K}. \quad (37)$$

This value is still large and cannot be negligible. In a similar way, the change in velocity can be estimated by neglecting the transport of momentum due to rain. Assuming that the momentum in a control volume is not changed, $U \equiv \rho u = \rho' u'$, and using a typical value, $u = 30$ m s^{-1}, we estimate the change in velocity as

$$\Delta u = u' - u = \frac{q_r}{1 - q_r} u \approx 10^{-3} \times 30 = 0.03 \text{ m s}^{-1}. \quad (38)$$

Since this is a small value, we may say that the effect of transport of momentum due to rain can be neglected for simplicity.

Finally, we summarize the energy budget of the above equations of the moist atmosphere following Ooyama (2001), for later diagnostics of numerical calculations. First, to derive the equation of kinetic energy, using the relation of Eqs. (29) and (30), the equations of momentum (31) and (32) are transformed to the advective form equations, and the inner product of the result with $\mathbf{v}$ gives the equation of kinetic energy $K = (u^2 + v^2 + w^2)/2$. Using again Eqs. (29) and (30), the flux form equation of kinetic energy is given by

$$\frac{\partial(\rho K)}{\partial t} + \nabla_H \cdot (\rho K \mathbf{v}_H) + \frac{\partial}{\partial z}[(\rho w + \rho q_r w_r)K] + \rho g w + \mathbf{v} \cdot \nabla p = 0. \quad (39)$$

The equation of potential energy $\rho d\Phi/dt = \rho g w$ is written in flux form as

$$\frac{\partial(\rho \Phi)}{\partial t} + \nabla_H \cdot (\rho \Phi \mathbf{v}_H) + \frac{\partial}{\partial z}[(\rho w + \rho q_r w_r)\Phi] = \rho g w + \rho q_r w_r g. \quad (40)$$

In general, since $w_r < 0$, the term $\rho q_r w_r g$ is a decrease of potential energy due to rain. Summing up Eqs. (39), (40), and (33), we obtain the equation of total energy:

$$\frac{\partial}{\partial t}[\rho(e + K + \Phi)] + \nabla_H \cdot \{[\rho(e + K + \Phi) + p]\mathbf{v}_H + \mathbf{F}_H\} + \frac{\partial}{\partial z}\{[\rho(e + K + \Phi) + p]w + \rho q_r(e_r + K + \Phi)w_r + F_z\} = 0. \quad (41)$$

Here, we have assumed that the diabatic heating is written as $Q'_H = -\nabla \cdot \mathbf{F}$, where the energy flux $\mathbf{F} = (\mathbf{F}_H, F_z)$ contains both the sensible and latent heat fluxes.

4. Time integration scheme

We use a numerical scheme that guarantees the conservation of mass, momentum, and energy based on the flux form equations. The treatment of the fast modes of sound waves and gravity waves follows the method described by Satoh (2002); that is, the vertically propagating waves are implicitly calculated while the horizontally propagating waves are explicitly calculated. This type of time integration scheme is denote as the horizontally explicit and vertically implicit (HEVI) scheme. The vertical component of momentum is solved implicitly with a one-dimensional Helmholtz equation,

and the density and the energy are solved using the conservative form equations. Satoh (2002) argues that there are choices of the prognostic variable in the stage of the integration of energy, and devised a conservative method that guarantees the conservation of total energy. We extend the ''conservative method'' proposed by Satoh (2002) and use the method in which the total energy is integrated in time (see below).

We adopt the time-splitting method in the flux form equations proposed by Klemp et al. (2000). In the time-splitting method, the fast modes related to sound waves and gravity waves are integrated with a small time step, while the other slow modes are integrated with a large time step (Klemp and Wilhelmson 1978; Skamarock and Klemp 1992). According to Klemp et al. (2000), the fluxes related to the fast modes are divided into the values at the large time step and the deviations from them.

We choose the prognostic variables ρ, $\rho\mathbf{v}_H$, ρw, ρe_a, ρq_v, ρq_c, and ρq_r. Denoting the deviations of pressure and density from their hydrostatic reference values by p' and ρ', we define the following symbols: $\mathbf{V} = (U, V, W) \equiv (\rho u, \rho v, \rho w)$, $P = p'$, $R = \rho'$, $E = \rho e_a$, and $(Q_v, Q_c, Q_l) = (\rho q_v, \rho q_c, \rho q_r)$. In the time-splitting method, the water substances (Q_v, Q_c, Q_l) are updated at large time steps. Only R, $\mathbf{V}_H$, W, E, and P are updated at small time steps, and the other quantities are kept constant during small time step integrations. The equations for (Q_v, Q_c, Q_l) are given by Eqs. (24), (25), and (26). The equations for R, $\mathbf{V}_H$, W, and E are given from Eqs. (28), (31), (32), and (35) as

$$\frac{\partial R}{\partial t} + \boldsymbol{\nabla}_H \cdot \mathbf{V}_H + \frac{\partial}{\partial z} W = -\frac{\partial}{\partial z}(Q_r w_r) \equiv G_R, \quad (42)$$

$$\frac{\partial \mathbf{V}_H}{\partial t} + \boldsymbol{\nabla}_H P = -\boldsymbol{\nabla}_H \cdot (\mathbf{V}_H \mathbf{v}_H) - \frac{\partial}{\partial z}(W\mathbf{v}_H) - \frac{\partial}{\partial z}(Q_r \mathbf{v}_H w_r) + \mathbf{F}_H \equiv \mathbf{G}_V, \quad (43)$$

$$\frac{\partial W}{\partial t} + \frac{\partial P}{\partial z} + Rg = -\boldsymbol{\nabla}_H \cdot (\mathbf{V}_H w) - \frac{\partial}{\partial z}(Ww) - \frac{\partial}{\partial z}(Q_r w w_r) + F_z \equiv G_W, \quad (44)$$

and

$$\frac{\partial E}{\partial t} + \boldsymbol{\nabla}_H \cdot (\mathbf{V}_H h_a) + \frac{\partial}{\partial z}(Wh_a) + \mathbf{v} \cdot \boldsymbol{\nabla}_p = -\frac{\partial}{\partial z}(Q_r e_r w_r) - Q_r w_r g + L_{00}(S_{\text{conv}} - S_{\text{evap}}) + Q_H \equiv G_E, \quad (45)$$

where the fast mode terms are placed on the left-hand side and the other slow-mode terms are on the right-hand side. Note that since the advection of density and enthalpy are related to the propagation of sound waves, these terms are counted as the fast modes.

We denote a large time step by t, a small time step by τ, and their intervals by Δt and $\Delta\tau$, respectively. Denoting values of a variable A at respective time steps by A^t and A^τ, we also write $\delta_\tau A = (A^{\tau+\Delta\tau} - A^\tau)/\Delta\tau$ and $A^{*\tau} = A^\tau - A^t$. We use the following time discretization for Eqs. (42), (43), (44), and (45):

$$\delta_\tau R^* + \boldsymbol{\nabla}_H \cdot \mathbf{V}_H^{*\tau+\Delta\tau} + \frac{\partial}{\partial z} W^{*\tau+\Delta\tau} = -\boldsymbol{\nabla}_H \cdot \mathbf{V}_H^t - \frac{\partial}{\partial z} W^t + G_R^t, \quad (46)$$

$$\delta_\tau \mathbf{V}_H^* + \boldsymbol{\nabla}_H P^{*\tau} = -\boldsymbol{\nabla}_H P^t + \mathbf{G}_V^t, \quad (47)$$

$$\delta_\tau W^* + \frac{\partial P^{*\tau+\Delta\tau}}{\partial z} + R^{*\tau+\Delta\tau} g = -\frac{\partial P^t}{\partial z} - R^t g + G_W^t, \quad (48)$$

and

$$\delta_\tau E^* + \boldsymbol{\nabla}_H \cdot (\mathbf{V}_H^{*\tau+\Delta\tau} h_a^t) + \frac{\partial}{\partial z}(W^{*\tau+\Delta\tau} h_a^t) + \overline{[\mathbf{v} \cdot \boldsymbol{\nabla} p]}^{*\tau} = -\boldsymbol{\nabla}_H \cdot (\mathbf{V}_H^t h_a^t) - \frac{\partial}{\partial z}(W^t h_a^t) - \mathbf{v}^t \cdot \boldsymbol{\nabla} p^t + G_E^t. \quad (49)$$

The expression of the term $\overline{[\mathbf{v} \cdot \boldsymbol{\nabla} p]}^{*\tau}$ will be described later according to the implicit treatment.

The horizontal momentum equations (47) are stepped forward explicitly, and the continuity equation (46) and the vertical momentum equation (48) are solved implicitly. The internal energy equation (49) is used to eliminate pressure from the vertical momentum equation, as describe below, but the internal energy itself is computed from a conservation equation for total energy that we will present shortly. Using $E = \rho e_a$ and Eqs. (22), (34), and (5), we have the relations

$$\frac{R_d}{C_{vd}} E = \frac{q_d C_{vd} + q_v C_{vv} + q_l C_l}{C_{vd}} \frac{R_d}{q_d R_d + q_v R_v} p \equiv \varepsilon_1 p_1 \quad (50)$$

and

$$\frac{R_d}{C_{vd}} h_a = \frac{q_d C_{pd} + q_v C_{pv} + q_l C_l}{C_{pd}} c_s^2 \equiv \varepsilon_2 c_s^2, \quad (51)$$

where $c_s^2 = (C_{pd}/C_{vd}) R_d T$ is the square of the sound wave speed in a dry atmosphere. In general, we have approximations, $\varepsilon_1 \approx 1$ and $\varepsilon_2 \approx 1$, under the conditions $q_d \approx 1$, $q_v \ll 1$, and $q_l \ll 1$. Multiplying Eq. (49) by R_d/C_{vd}, we can obtain the pressure equation as

$$\delta_\tau(\varepsilon_1 P)^* + \boldsymbol{\nabla}_H \cdot [\mathbf{V}_H^{*\tau+\Delta\tau}(\varepsilon_2 c_s^2)^t] + \frac{\partial}{\partial z}[W^{\tau+\Delta\tau}(\varepsilon_2 c_s^2)^t] + \frac{R_d}{C_{vd}} \overline{[\mathbf{v} \cdot \boldsymbol{\nabla} p]}^{*\tau} = \frac{R_d}{C_{vd}} [\text{rhs of (49)}]. \quad (52)$$

If we consider a propagation of linear sound waves, the

advection of $\varepsilon_2 c_s^2$ on the left-hand side is counted as that of the basic field. This indicates that the value of $\varepsilon_2 c_s^2$ can be evaluated at the large time step. Similarly, the term $[\mathbf{v}\cdot\nabla p]^{*\tau}$ is an effect of stratification on sound waves. Since the effect of horizontal variation of stratification is generally smaller than that of vertical variation, we may approximate this term according to the concept of linearization as

$$\overline{[\mathbf{v}\cdot\nabla p]}^{*\tau} = W^{\tau+\Delta\tau}\left[g - \frac{1}{\rho^t}\left(\frac{\partial P^t}{\partial z} + R^t g\right)\right] \equiv W^{\tau+\Delta\tau}\tilde{g}^t. \quad (53)$$

Thus, Eqs. (46), (48), and (52) construct simultaneous linear equations for $R^{*\tau+\Delta\tau}$, $W^{*\tau+\Delta\tau}$, and $P^{*\tau+\Delta\tau}$. We rearrange these equations as

$$\delta_\tau R^* + \frac{\partial}{\partial z}W^{*\tau+\Delta\tau} = -\nabla_H\cdot\mathbf{V}_H^{*\tau+\Delta\tau} - \nabla_H\cdot\mathbf{V}_H^t - \frac{\partial}{\partial z}W^t + G_R^t \equiv G_R'^{\tau+\Delta\tau}, \quad (54)$$

$$\alpha\delta_\tau W^* + \frac{\partial P^{*\tau+\Delta\tau}}{\partial z} + R^{*\tau+\Delta\tau}g = -\frac{\partial P^t}{\partial z} - R^t g + \alpha G_W^t, \quad \text{and} \quad (55)$$

$$\delta_\tau P^* + \frac{\partial}{\partial z}\left(W^{\tau+\Delta\tau}\frac{R_d}{C_{vd}}h_a^t\right) + \frac{R_d}{C_{vd}}W^{\tau+\Delta\tau}\tilde{g}^t = -\nabla_H\cdot\left(\mathbf{V}_H^{*\tau+\Delta\tau}\frac{R_d}{C_{vd}}h_a^t\right) + \frac{R_d}{C_{vd}}[\text{rhs of (49)}] \equiv \frac{R_d}{C_{vd}}G_E'^{\tau+\Delta\tau}, \quad (56)$$

where we set $\varepsilon_1 = \varepsilon_2 = 1$ and introduce the hydrostatic switch $\alpha = 0$ or 1. A single equation for either $P^{*\tau+\Delta\tau}$, $W^{*\tau+\Delta\tau}$, or $R^{*\tau+\Delta\tau}$ can be obtained from the above three equations. We choose the equation for $W^{*\tau+\Delta\tau}$, which enables us to easily introduce the hydrostatic option $\alpha = 0$; that is,

$$-\frac{\partial^2}{\partial z^2}\left(\Delta\tau^2\frac{R_d}{C_{vd}}h_a^t W^{*\tau+\Delta\tau}\right) - \left[\frac{\partial}{\partial z}\left(\Delta\tau^2\frac{R_d}{C_{vd}}\tilde{g}^t W^{*\tau+\Delta\tau}\right) + \Delta\tau^2 g\frac{\partial}{\partial z}W^{*\tau+\Delta\tau}\right] + \alpha W^{*\tau+\Delta\tau} = \alpha W^{*\tau} + \Delta\tau\left(-\frac{\partial P^t}{\partial z} - R^t g + \alpha G_W^t\right) - \Delta\tau\frac{\partial}{\partial z}\left[P^{*\tau} + \Delta\tau\frac{R_d}{C_{vd}}G_E'^{\tau+\Delta\tau}\right] - \Delta\tau g[R^{*\tau} - \Delta\tau G_R'^{\tau+\Delta\tau}]. \quad (57)$$

This can be solved for $W^{*\tau+\Delta\tau}$ with the boundary conditions at the bottom and the top of the atmosphere. The density $R^{*\tau+\Delta\tau}$ is calculated in flux form by substituting $W^{*\tau+\Delta\tau}$ into Eq. (54). Although the pressure $P^{*\tau+\Delta\tau}$ can also be calculatable from Eq. (56), several approximations are introduced to derive Eq. (56) so that the exact conservation of total energy no longer holds; thus, we need to introduce an energy correction.

Satoh (2002) compared various methods for the energy integration and found that the conservation of total energy is well satisfied if the sum of internal energy and kinetic energy is integrated in the small time step. Satoh (2002) denoted this method as the conservative method. We can use this method for the time integration of energy in the small time step, instead of Eq. (56), to obtain the internal energy $E^{\tau+\Delta\tau}$ and thus the pressure $P^{\tau+\Delta\tau}$. Summing up Eqs. (35) and (39), and introducing the time-splitting technique consistent with the above HEVI method, we obtain the equation for the sum of internal energy and kinetic energy:

$$\delta_\tau(E + \rho K) + \nabla_H\cdot[(h_a + K)^t\mathbf{V}_H^{\tau+\Delta\tau}] + \frac{\partial}{\partial z}[(h_a + K)^t W^{\tau+\Delta\tau}] + gW^{\tau+\Delta\tau} = \left\{-\frac{\partial}{\partial z}[Q_r(e_r + K)w_r] + Q_r w_r g + L_{00}(S_{\text{conv}} - S_{\text{evap}}) + Q_H\right\}^t. \quad (58)$$

This can be integrated for $E + \rho K$ at the time step $\tau + \Delta\tau$. Since the density and the three components of momentum at $\tau + \Delta\tau$ are already known, we can calculate the kinetic energy $(\rho K)^{\tau+\Delta\tau}$. Thus, the internal energy $E^{\tau+\Delta\tau}$ is determined. Here, we can extend the above method to use the total energy as a prognostic variable in this stage, such that

$$\delta_\tau(E + \rho K + \rho\Phi) + \nabla_H\cdot[(h_a + K + \Phi)^t\mathbf{V}_H^{\tau+\Delta\tau}] + \frac{\partial}{\partial z}[(h_a + K + \Phi)^t W^{\tau+\Delta\tau}] = \left\{-\frac{\partial}{\partial z}[Q_r(e_r + K + \Phi)w_r] + L_{00}(S_{\text{conv}} - S_{\text{evap}}) + Q_H\right\}^t. \quad (59)$$

TABLE 2. List of the squall-line experiments. Here, x_{max} is horizontal length. The colume labeled thermodynamics represents the treatment of the moist thermodynamics, where exact indicates the exact expressions with the effects of the specific heats of water substance and dependency of latent heat on temperature and simple indicates the simplified expressions by neglecting these effects. Here, γ is the factor for the coefficient of the horizontal numerical diffusion, Δt is the large time step, and N_s is the number of the time splitting.

Expt	x_{max} (km)	Thermo-dynamics	Δt (s)	γ	N_s
CTL100	100	Exact	1.5	0.015	1
SPL100	100	Simple	1.5	0.015	1
G05	100	Exact	1.5	0.005	1
G02	100	Exact	1.5	0.002	1
NS10	100	Exact	1.5	0.015	10
NS6-dt9	100	Exact	9.0	0.090	6
CTL1000	1000	Exact	1.5	0.015	1
SPL1000	1000	Simple	1.5	0.015	1

As shown by Satoh (2002), $gW^{\tau+\Delta\tau}$ on the left-hand side of Eq. (58) is the conversion term with the potential energy [see Eq. (40)]. However, it is found that this form of discretization causes a small error in the conservation of total energy if the terrain-following coordinate is used; this characteristic is not pointed out by Satoh (2002). This error can be avoided by integrating the above flux form of total energy.

To conclude this section, we summarize the time integration procedure. We use the leapfrog scheme for the large time step integration. The time filter is used to suppress the numerical mode. The leapfrog time step interval is denoted by $2\Delta t$, and each large time step integration is divided by the small time step interval $\Delta\tau$. The number of the time splitting is denoted by $N_s = 2\Delta t/\Delta\tau$.

1) Calculation of the tendency terms of the dynamical equations at a large time step t: the right-hand sides on Eqs. (46)–(49) are evaluated.
2) Time integration for U, V, W, R, and E with a small time step interval $\Delta\tau$ for N_s times from the values at $t - \Delta t$ to obtain the values at $t + \Delta t$:
   (i) explicit time integration of the horizontal components of momentum U and V using Eq. (47),
   (ii) implicit time integration of the vertical component of momentum W by solving Eq. (57) with the boundary conditions,
   (iii) integration for density R using the conservative form Eq. (54), and
   (iv) the energy correction step for the evaluation of internal energy E under the constraint of the total energy conservation Eq. (59).
3) Integration of the water substances for the time step $t + \Delta t$: the tendency terms in Eqs. (24)–(26) are evaluated. At this stage, we set $S_{conv} = 0$.
4) The adjustment process: temperature T is given by Eq. (20) using an iterative method from e, ρ, and q_m, where $\rho = \rho_s + R$, $e = E/\rho$, and $q_m = Q_m/\rho$. The water vapor q_v and the cloud water q_c are given by Eq. (17).
5) Using a time filter, the values at t are updated from the values at $t - \Delta t$ and $t + \Delta t$.

5. Model and results

a. Numerical model

We have developed a numerical model based on the scheme stated in the previous section. The model is constructed in the three-dimensional Cartesian coordinates, although we will only show the numerical results in the two-dimensional calculation. The thermodynamic variables R, E, P, and Q_i are defined at the same points, and the three components of momentum U, V, and W are defined at the staggered points in the x, y, and z directions, respectively; that is, the Arakawa C grid is used. In the vertical, the Lorenz grid is used. The top and the bottom of the atmosphere are rigid and periodicity is assumed at the lateral boundaries. The temporal scheme is summarized in the last paragraph of the previous section. The advection scheme of the water substance is the third-order upstream scheme, and the second-order central scheme is used for the advections of the other variables. For the transports due to rain, we introduce a higher-order advection scheme with the conservative semi-Lagrangian (CSL) method (Xiao and Yabe 2001; Xiao et al. 2003).

The fourth-order Laplacian horizontal numerical diffusion and the Rayleigh damping are introduced for the three components of velocity and temperature. The coefficient of the numerical diffusion is given as

$$\nu = \gamma\frac{\Delta x^4}{\Delta t} \quad \mathrm{m^4\ s^{-1}}, \tag{60}$$

where $\gamma = 0.015$ is used as the standard value. The Rayleigh damping is applied in the one-third depth from the top with a constant relaxation time $\tau_R = 10\Delta t$. The coefficient of the time filter for the leapfrog scheme is 0.05.

b. Experimental setup

We perform numerical experiments for a squall line following Redelsperger et al. (2000) and examine the numerical results particularly in terms of the conservation of water and energy. The main purpose of the numerical calculations in this study is to show the conservation of these quantities with the introduction of the moist processes. We use the minimum physical processes; only the warm rain is introduced as the cloud physics (Klemp and Williamson 1978; Ooyama 2001), and no ice phase is considered. The radiation, turbulence, and boundary processes are not introduced in these experiments.

Although both the two- and three-dimensional calculations are proposed by Redelsperger et al. (2000),

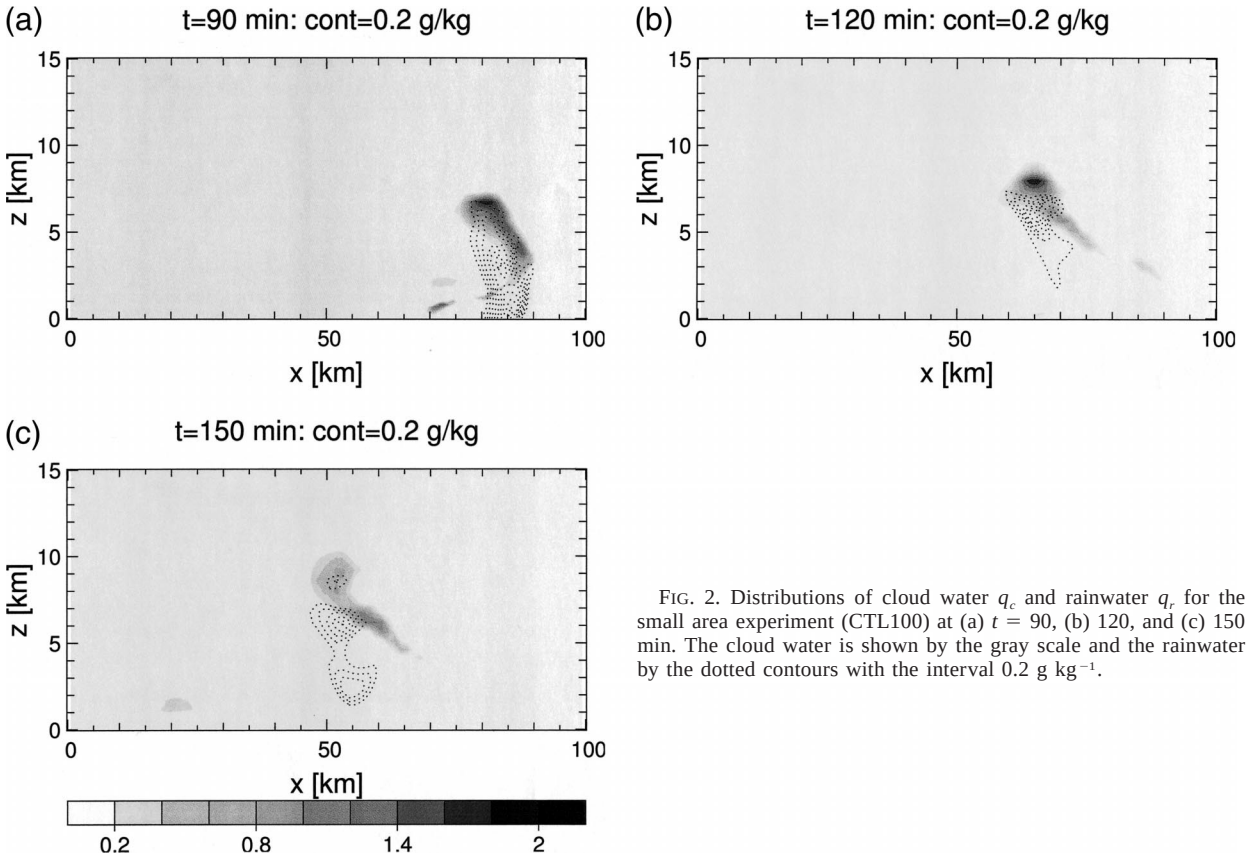

FIG. 2. Distributions of cloud water q_c and rainwater q_r for the small area experiment (CTL100) at (a) $t = 90$, (b) 120, and (c) 150 min. The cloud water is shown by the gray scale and the rainwater by the dotted contours with the interval 0.2 g kg^{-1}.

we concentrate on the two-dimensional calculation. The domain to be examined is 100 km in the lateral length and 21 km in the vertical direction, and the duration of integration is 7 h. Vertical profiles of temperature, specific humidity, and horizontal winds (u, v) are given as the initial conditions based on the observation of the Tropical Ocean Global Atmosphere Coupled Ocean–Atmosphere Response Experiment (TOGA COARE). In addition, in order to keep the squall line at almost the same position, uniform winds of $U_0 = -12$ m s^{-1} and $V_0 = 2$ m s^{-1} are also applied. The squall line is initiated by an initial forcing for the first 20 min by cooling and drying at $x = 85$ km and $z \leq 2.5$ km with lateral width $r = 7$ km. The amplitudes are -6.7 K s^{-1} for the cooling rate and -1.675×10^{-6} kg kg^{-1} s^{-1} for the drying rate.

Redelsperger et al. (2000) proposed the use of the open lateral boundary condition in order to avoid the effect of the lateral boundaries. However, it is not ap-

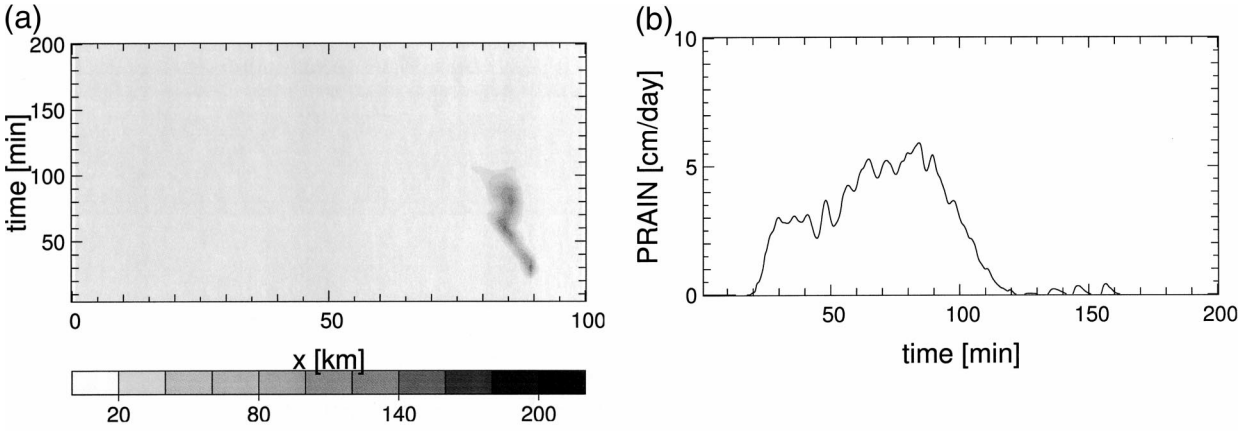

FIG. 3. (a) Evolution of the horizontal distribution of precipitation in the x–t domain and (b) time sequence of the total precipitation for the small area experiment (CTL100). Units are cm day^{-1}.

propriate for our purpose; in order to examine the conservation of physical quantities, simulations in a well-defined domain are preferable. Thus, we extend the lateral length to 1000 km to compare with the results shown by Redelsperger et al. (2000). In addition, we also perform the small area experiments with 100-km length in order to investigate dependencies on various experimental parameters. As shown below, or as is well known, the behavior of a squall line in the small area experiments is very different from that in the large area experiments with the domain length of 1000 km: the cloud system associated with the squall line does not continue in the case of the small area experiments; only a single cloud is produced. Although this behavior is unrealistic, the deterministic evolution of the cloud is useful for the study of the sensitivity of the model.

The horizontal grid interval is $\Delta x = 1.25$ km, and the stretched grid interval is used in the vertical. The number of grid points is 800×44 in the 1000-km-length experiment and is 80×44 in the small area experiments. For the standard experiments, we do not use the time splitting, $N_s = 1$, and we set the time step intervals as $2\Delta t = \Delta\tau = 3.0$s. The effect of the number of the time-splitting N_s will be examined in the small area experiments. All the experiments are summarized in Table 2.

We will diagnose the numerical results in terms of the following budget equations. In these experiments, no supply of vapor and energy is allowed from the surface, but the initial forcing of vapor and temperature is given. The budget of the column-integrated water averaged over the total domain is written as

$$\Delta\frac{1}{x_{\max}}\int_0^{x_{\max}}\int_0^{z_{\top}}\rho(q_v + q_c + q_r)\,dz\,dx = -\frac{1}{x_{\max}}\int_0^{t}\int_0^{x_{\max}}P_r\,dx\,dt + \frac{1}{x_{\max}}\int_0^{t}\int_0^{x_{\max}}\int_0^{z_{\top}}\rho S\,dz\,dx\,dt, \quad (61)$$

where $x_{\max} = 100$ or 1000 km, $z_{\top} = 21$ km, Δ is the difference from the initial state, $P_r = -\rho q_r w_r(z = 0)$ is the precipitation rate at the surface, and S is the forcing term of vapor ($S < 0$). The budget of the column-integrated energy is written as

$$\Delta\frac{1}{x_{\max}}\int_0^{x_{\max}}\int_0^{z_{\top}}\rho(e_a + L_{00}q_v + K + \Phi)\,dz\,dx = -\frac{1}{x_{\max}}\int_0^{t}\int_0^{x_{\max}}F_r\,dx\,dt + \frac{1}{x_{\max}}\int_0^{t}\int_0^{x_{\max}}\int_0^{z_{\top}}\rho(Q_H + L_{00}S)\,dz\,dx\,dt, \quad (62)$$

where Q_H is the diabatic term due to the initial forcing. The outflow of energy due to rain at the surface is designated by $F_r = -\rho q_r(e_r + K + \Phi)w_r$. We will compare the numerical results using the exact formulation of thermodynamics and those using the simplified thermodynamics as described in section 2. If the simplified thermodynamics are used, the latent heat L_{00} is replaced by L_0 and the value of e_r is set equal to e_a in the transport of energy due to rain.

c. Small area experiments (100 km)

First, we show the results of the small area experiment with $x_{\max} = 100$ km using the exact formulation of the thermodynamics. This experiment is denoted as the control experiment and is referred to as CTL100. The snapshots of cloud water and rainwater at times $t = 90$, 120, and 150 min are shown in Fig. 2. The cloud is generated near the place where the initial forcing is applied at $x = 85$ km and it ascends with drifting downstream. (Note that the zonal wind $U_0 = -12$ m s^{-1} is added in the domain.) The time variability of precipitation at the surface is depicted in Fig. 3a for the time evolution of the horizontal distribution and in Fig. 3b for the time sequence of the total precipitation. A strong precipitation is observed up to $t = 90$ min. But the rainwater does not reach the surface afterward; most of the rainwater is evaporated in the lower layers and the cold pool is formed at the downstream side of the cloud (figures are not shown). If the domain length is larger, a second cloud is generated by the outflow of the cold pool and the squall line is maintained. In this experiment, however, since the domain length is too small, the updraft of a successive cloud is prohibited by the downward motion of the preceding cloud so that the cloud system decays rapidly. This behavior of development of cloud is different from that in the 100-km experiment with the open boundary condition in Redelsperger et al. (2000) (see Fig. 4a in their paper for the ''C_2D_MRI'' case). In the next subsection, in order to avoid the effect of the lateral boundary, we perform the large area experiment at 1000 km. The results of Redelsperger et al. (2000) should be compared with those of the next section.

The water and the energy budgets of the control experiment (CTL100) are shown in Fig. 4. These are cumulative values per unit area averaged over the domain according to Eqs. (61) and (62). In Fig. 4a, the time sequence of the water budget shows each term of Eq. (61): change in vapor q_v, change in liquid water $q_c + q_r$, change in the total water $q_w = q_v + q_c + q_r$, cumulative value of precipitation P_r, and cumulative value of the initial forcing S. The curve denoted by ''total'' is the difference between the two sides of Eq. (61), and must be equal to zero if the budget of the model is correct. As shown by Fig. 4a, the change in the total water q_w is almost equal to the cumulative value of the precipitation, so that the total budget is almost equal to zero. That is, the conservation of the water is confirmed in this model. The energy budget is shown in Fig. 4b,

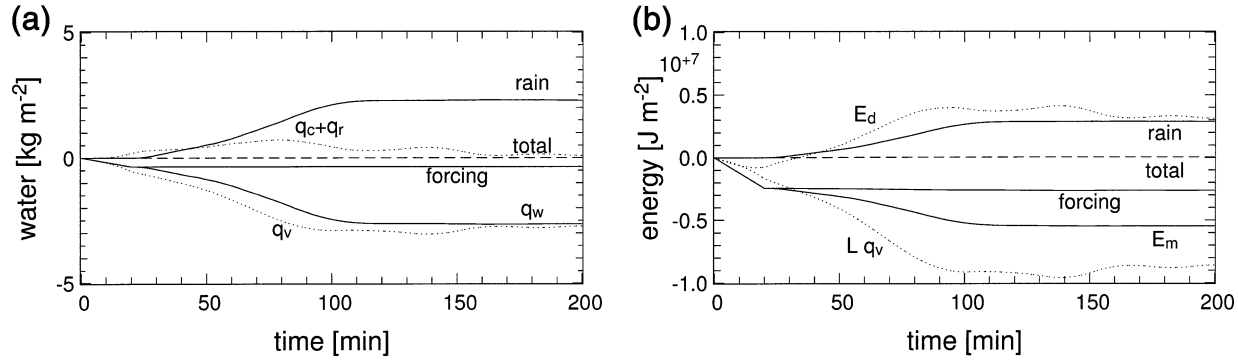

FIG. 4. (a) The water budget and (b) the energy budget for the small area experiment (CTL100) shown by column-integrated values per unit area. The values are differences from the initial values or cumulative values in time. In (a), q_v is water vapor (dotted), $q_c + q_r$ is the sum of cloud water and rainwater (dotted), q_w is the total water (solid), rain is the outflow into the surface due to rain (solid), forcing is the change due to the initial forcing (solid), and total is the total water budget (dashed). In (b), E_d is the dry total energy (dotted), Lq_v is the latent heat (dotted), E_m is the moist total energy (solid), rain is the outflow into the surface of energy due to rain (solid), forcing is the change due to the initial forcing (solid), and total is the total energy budget (dashed).

where $E_d = e_a + K + \Phi$ and $E_m = E_d + L_{00}q_v$, where E_d may be viewed as the total energy of the dry air and E_m is that of the moist air including the effect of latent heat. As shown by the figure, the contribution of the initial forcing is relatively larger in this experiment. The change in E_m is almost equal to the sum of the outflow of energy due to rain and the initial forcing. The total budget designated by ''total'' is almost zero.

The results of the above experiment can be compared with those of SPL100 where the simplified thermodynamics are used. Figure 5 shows the time sequence of precipitation. The precipitation of SPL100 is generally larger than that of CTL100 (Fig. 3b). In general, the cloud motion is more intense and the cloud reaches higher levels in the case of SPL100 (figures are not shown). Figure 6 shows the water budget and the energy budget of SPL100. The quantitative difference of the total precipitation can be clearly indicated if compared with Fig. 4a. The domain-averaged cumulative value of the precipitation is 2.28 mm for CTL100, while it is 2.60 mm for SPL100. The total rain is overestimated by about 14% if the simplified thermodynamics are used. As for the energy budget, since the specific heat of liquid water is neglected, the energy transport due to rain is small. Note that in this case the energy transport due to rain is calculated by using the specific heat of the dry air [see the comments below Eq. (33)], the energy transport due to rain in CTL100 is about $C_l/C_{vd} = 5.87$ times of that in SPL100. Thus, the change in the moist energy E_m is almost equal to the initial forcing of energy in the case of SPL100. The definition of the latent heat designated by Lq_v is also different between the two cases; in CTL100, it is defined as $L_{00}q_v$, while in SPL100 it is defined as L_0q_v. Although the change in the dry total energy E_d of SPL100 is larger than that of CTL100, there is little difference in the change in the latent heat between the two cases. The difference in the latent heat $L_{00}/L_0 = 1.25$ is reflected in the change in the vapor content. In the case of SPL100, most of the latent heat release is used for the increase in the dry total energy E_d. In the case of CTL100, however, since the energy transport due to rain is not negligible, the dry total energy is not greatly increased even if the equal amount of the latent heat is released.

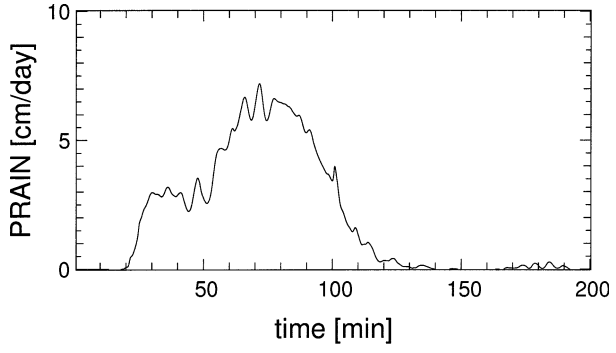

FIG. 5. The same as in Fig. 3b but for the experiment SPL100.

The dependency of the precipitation on other experimental parameters is compared in Fig. 7. All the results are characterized by the evolution of a single cloud similar to CTL100 (Fig. 3b) and SPL100 (Fig. 5). First, the dependency on the horizontal numerical diffusion is shown in Figs. 7a and 7b. The horizontal numerical diffusion is controlled by the value of γ in Eq. (60). As can be seen from Figs. 7a and 7b, as γ becomes smaller, a sporadic intense precipitation tends to occur. This result is not surprising since we do not introduce any realistic turbulent models.

In Figs. 7c and 7d, the effect of the number of time-splitting N_s is shown; Fig. 7c is for $N_s = 10$ and $\Delta t = 1.5$ (s), while Fig. 7d is for $N_s = 6$ and $\Delta t = 9.0$ (s). The large time step Δt in Fig. 7c is the same as that in CTL100, and the small time step $\Delta\tau$ of Fig. 7d is the

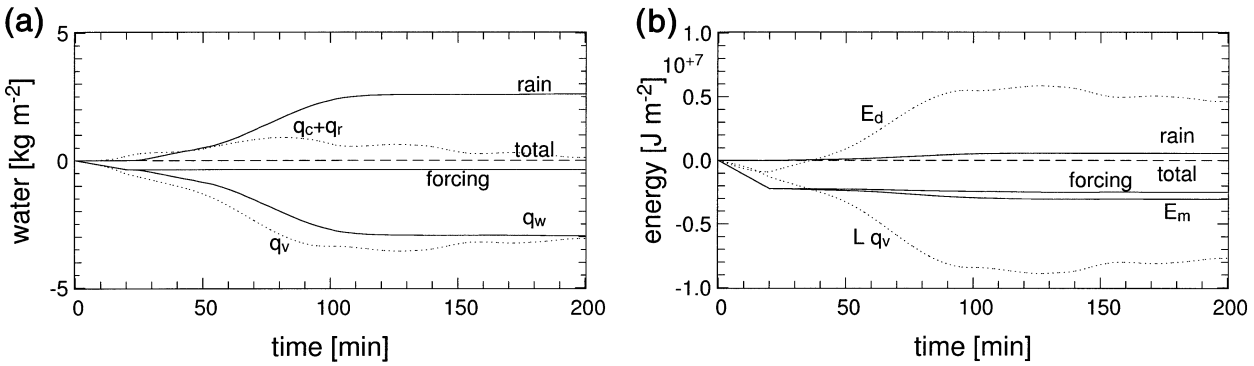

FIG. 6. The same as in Fig. 4 but for the experiment SPL100.

same as that in CTL100. In these experiments, the numerical diffusion ν in Eq. (60) is kept constant by choosing the coefficient γ proportional to Δt (see Table 2). We use the divergence damping, whose coefficient is given by $\alpha_D = 0.05 c_s^2 \Delta\tau$ (Skamarock and Klemp 1992). The first message from these results is that our scheme is stable for the time splitting even for $N_s = 6$ and 10. In particular, if the large time step Δt is kept constant as for Fig. 7c, the model should run for any large number of the splitting N_s since the Courant conditions are always satisfied. In contrast, if the small time step $\Delta\tau$ is kept constant as for Fig. 7d, the number of the splitting N_s is limited; if we use a further increased number of N_s, say $N_s = 8$, the numerical integration cannot be continued; it is because the Courant number of the vertical advection for the large time step exceeds one. In both Figs. 7c and 7d, the precipitation is enhanced in comparison to CTL100. In particular, as shown by Fig. 7d, the precipitation increases as N_s is increased with keeping $\Delta\tau$ constant. In the case of Fig. 7d, since the Courant number is closer to one, the computation is marginally stable and the vertical velocity is relatively overestimated. Such a dependency on the number of the time-splitting N_s is worth noticing. This kind of model

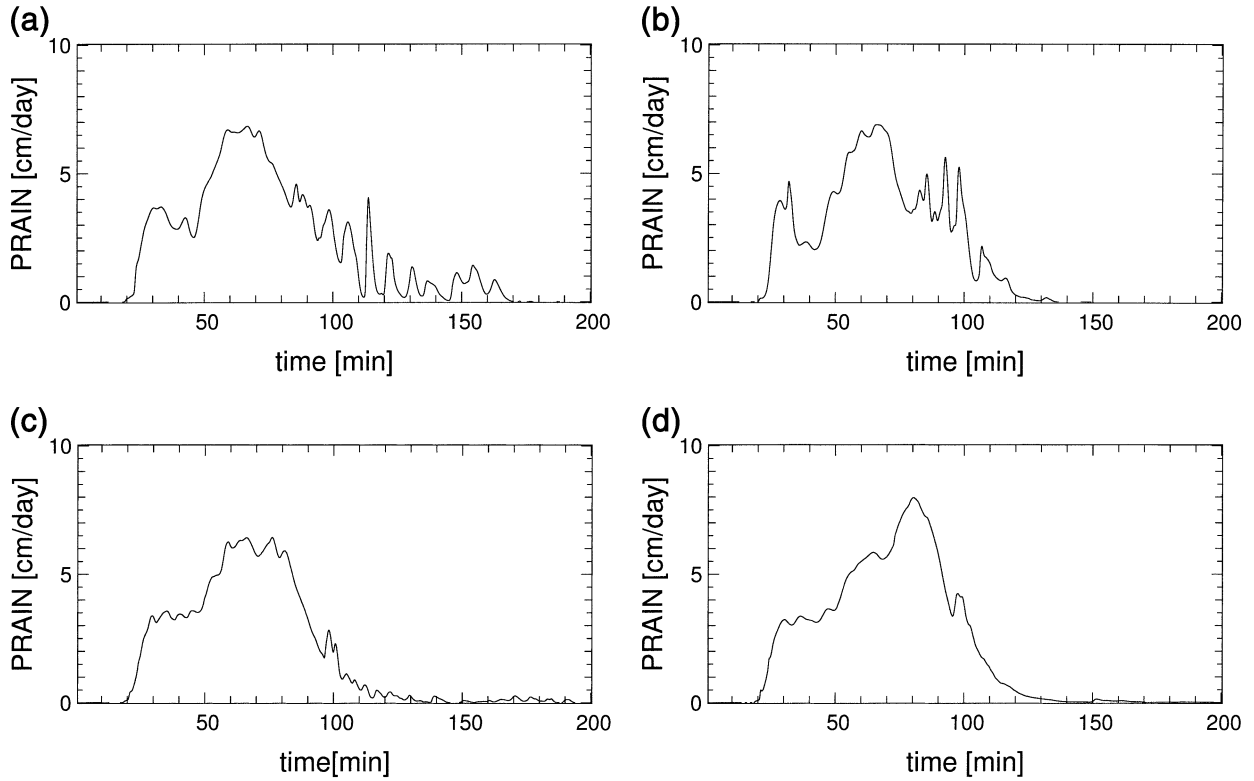

FIG. 7. The same as in Fig. 3b but for the experiments (a) G05, (b) G02, (c) NS10, and (d) NS6-dt9.

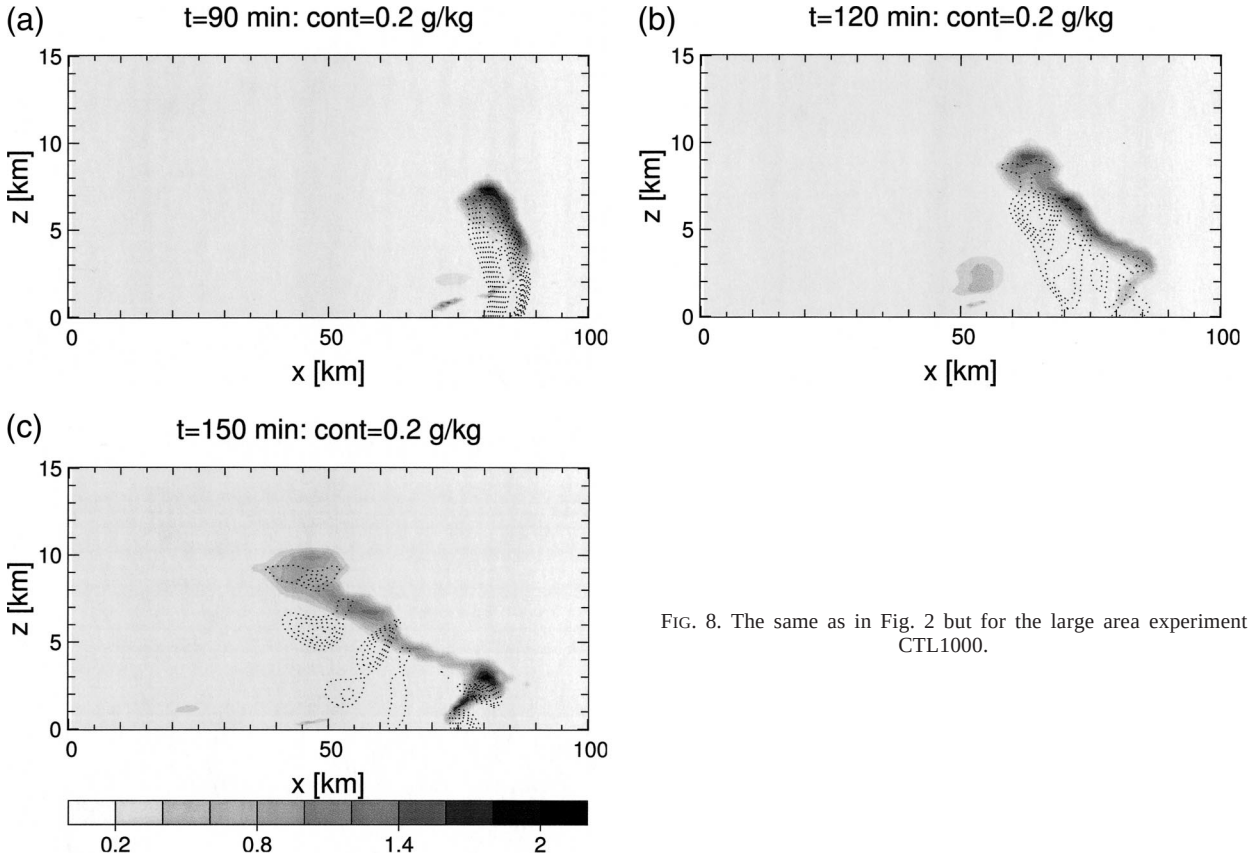

FIG. 8. The same as in Fig. 2 but for the large area experiment CTL1000.

variability totally depends on the appropriate choice of turbulent models; the problem concerning the choice of turbulent models is out of the range of the present work.

d. Large area experiments (1000 km)

In the next step, the horizontal length is extended to the range $0 \leq x \leq 1000$ km ($x_{max} = 1000$ km). The initial forcing is applied at the same place, $x = 85$ km, as in the small area experiments. The comparison with the small area experiments should be made within the range $0 \leq x \leq 100$ km. Figure 8 shows the distribution of cloud water and rainwater at $t = 90$, 120, and 150 min, and Fig. 9a shows the time evolution of the horizontal distribution of precipitation for the case with the exact thermodynamics (CTL1000). Unlike the small

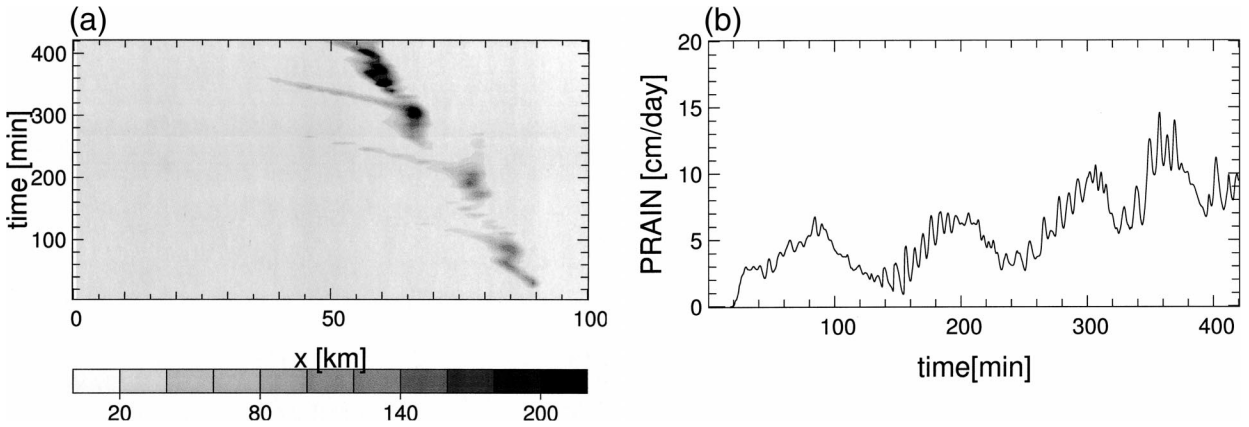

FIG. 9. The same as in Fig. 3 but for the large area experiment CTL1000. In (b), the precipitation is not averaged over the total domain, but over the region $x = 0$–100 km.

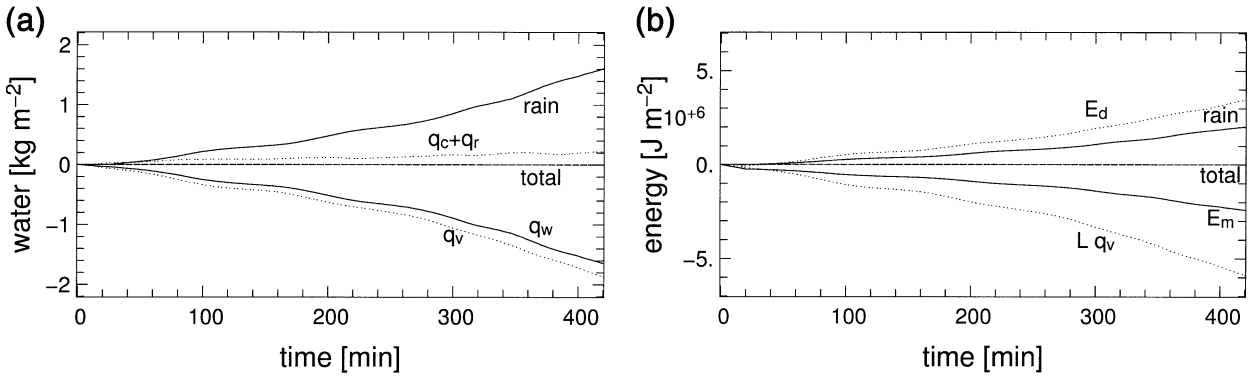

FIG. 10. The same as in Fig. 4 but for the large area experiment CTL1000. The forcing terms are omitted.

area experiments, here the squall line is maintained and drifts downstream during this time integration. The precipitation occurs within the range $0 \leq x \leq 100$ km. Figure 9b shows the time sequence of the total rain averaged over $x = 0$–100 km. The first peak around $t = 80$ min corresponds to the precipitation seen in the small area experiments (Fig. 3 for CTL100). The successive clouds have stronger peaks of precipitation.

Figure 10 shows the water budget and the energy budget for CTL1000 based on Eqs. (61) and (62). Here, we omit the curves for the initial forcing due to S and Q_H; these are very small and about 1/10th of those of CTL100, as shown in Fig. 4. The water budget shows that the change in the total water q_w is almost equal to the cumulative value of the precipitation and that the total budget is nearly equal to zero. The energy budget also shows that the energy outflow due to rain is almost equal to the change in the moist total energy E_m. Thus, we have confirmed again in this large area experiment that this model guarantees the conservation of water and total energy.

Figure 11 shows the vertical distributions of zonal wind, vertical wind, liquid water, and the deviation of potential temperature for the time average over $t = 5$–6 h and the spatial average over $x = 0$–100 km. These should be compared with those of Redelsperger et al. (2000). The zonal wind (Fig. 11a) indicates that the lower shear is strengthened and an oscillatory structure appears above the jet; these are similar characteristics to Fig. 12 of Redelsperger et al. The vertical wind (Fig. 12b) takes a maximum value about 0.14 m s^{-1} near $z = 6$ km. This height is slightly higher than those in Fig. 14 of Redelsperger et al. but the magnitude is almost comparable. Our rainwater and the total liquid water shown by Fig. 11c is within the variability shown by Figs. 16 and 17 of Redelsperger et al. The deviation of potential temperature θ' (Fig. 11d) shows that the cold pool is established in the lower layer. In particular, it is about -1 K just above the surface. Note that the surface energy flux is not introduced in this experimental setup.

The precipitation for the case with the simplified thermodynamics (SPL1000) is shown in Fig. 12. In comparison to CTL1000 (Fig. 9), the downstream drift of the squall line ceased until $t = 200$ min; after that, the squall line propagated upstream. The total precipitation is larger than that in CTL1000. Actually, the decrease in the total vapor q_v is 1.86 kg m^{-2} for CTL1000, while it is 2.41 kg m^{-2} for SPL1000. It is also shown in the large area experiments that the precipitation of the simplified thermodynamics is larger than that of the exact thermodynamics. The time sequence of the precipitation shows a large fluctuation with the time period of about a few minutes. A similar fluctuation is also seen in CTL1000, but the amplitude is much larger in this case. Since it is found that this fluctuation is sensitive to the numerical diffusion, it might no longer exist if a realistic turbulent model is introduced.

6. Summary and discussion

We have proposed a new numerical scheme for the fully compressible nonhydrostatic model including moist processes. The numerical scheme is based on the flux form equations of densities of water substance, total density, three components of momentum, and total energy, and the domain integrals of these variables are conserved. A time-splitting scheme is used with a leapfrog scheme for the large time step integration. The fast mode related to sound/gravity waves is treated implicitly for the vertical propagation and explicitly for the horizontal propagation. Following Satoh (2002), the implicit calculation is solved for the vertical momentum first, and then integrated for density and total energy using the flux form discretized equations.

We particularly proposed a method for the incorporation of moist processes. Although our scheme is similar to Ooyama (1990, 2001), there is a difference in that our scheme satisfies the conservation of total energy. As a quantitative improvement over conventional nonhydrostatic models, we use an exact formula of the moist thermodynamics considering the effects of the specific heats of water substance and the temperature dependency of the latent heat. The transports of mass, momentum, and energy due to rain are appropriately

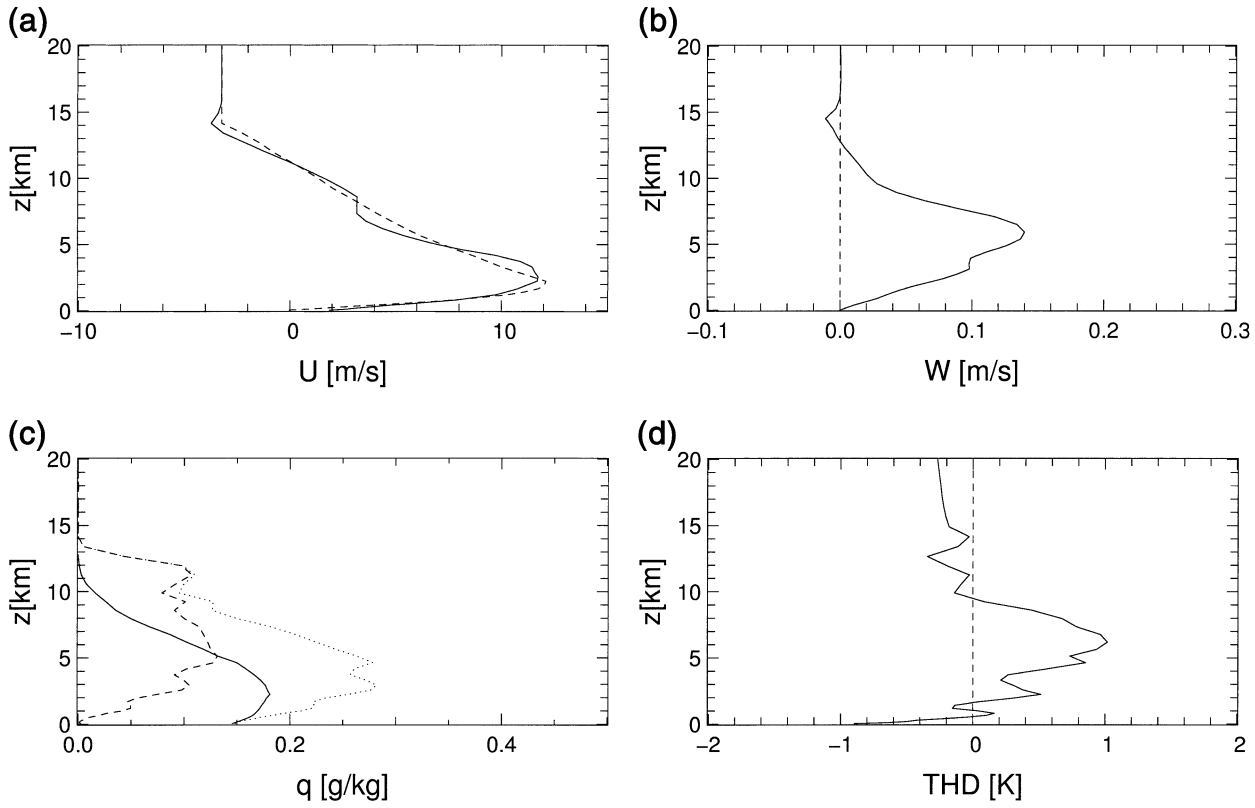

FIG. 11. Vertical distributions of (a) zonal wind (dotted curve is the initial profile), (b) vertical wind, (c) cloud water (dashed), rainwater (solid), and the sum of the two (dotted), and (d) deviation of potential temperature for the large area experiment (CTL1000) averaged over the time $t = 5$–6 h and the domain $x = 0$–100 km. Units are m s^{-1} in (a), (b), kg kg^{-1} in (c), and K in (d).

introduced following Ooyama (2001), and an accurate higher-order advection scheme is used for these transports. It is estimated that the effects of the transport of energy due to rain are not negligible, while those of momentum are generally small and might be negligible.

The applicability of the new numerical scheme is tested with two-dimensional experiments of a squall line. The experiments are performed at both 100- and 1000-km horizontal lengths with the horizontal grid interval of 1.25 km. It is found that the conservation of water and energy is well satisfied in these experiments. In the small area experiments of 100-km length, only a single cloud is developed and the squall line does not continue after the decay of the first cloud. Although this behavior is unrealistic, it is useful for comparison of the model performance since the evolution of the cloud is in a

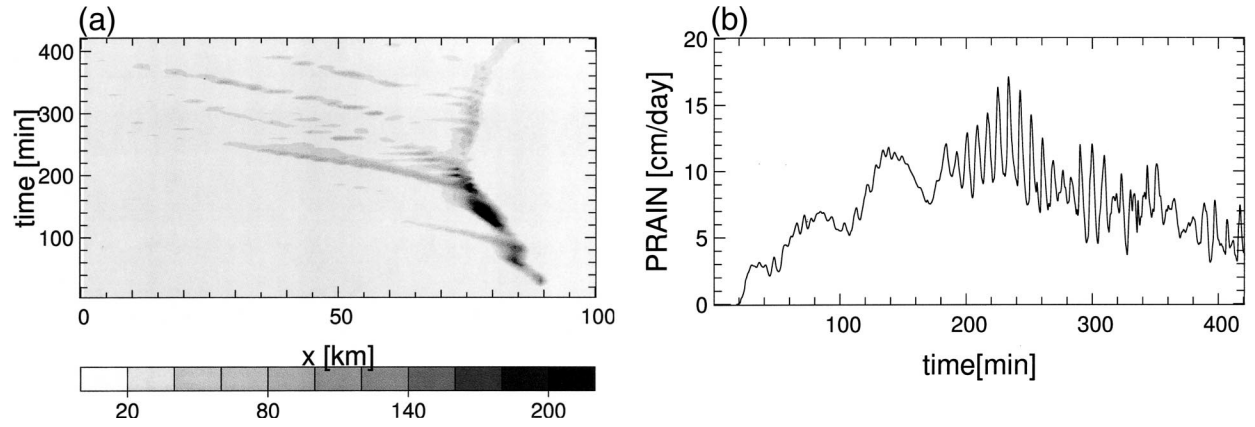

FIG. 12. The same as in Fig. 9 but for the large area experiment SPL1000.

deterministic regime. Dependency on the numerical diffusion ν and the number of time-splitting N_s is investigated. The model results show that variability of precipitation is appreciably affected by ν and N_s. These dependencies will be controlled by an appropriate choice of the turbulence model.

We particularly examined the effect of the treatment of the moist thermodynamics. It is found that, if the exact expressions of the thermodynamics are used, the total precipitation is reduced more than 10% in comparison to the case when the conventional simplified expressions are used. The results with the large area experiments with 1000-km horizontal length have many similarities to those of the preceding studies; evolutions of cloud system and vertical distributions of physical quantities are compared. The squall line continues for more than 7 h by successive development of clouds. The effect on the treatment of the moist thermodynamics is enhanced in such a longer time integration. If the simplified thermodynamics are used, the direction of the propagation of the squall line is reversed to the upwind direction at 4 h in the integration.

One of the characteristics of the new numerical scheme is the use of the flux form equation for total energy. It should be noted, however, that this choice does not necessarily lead to accuracy in the numerical results. In fact, numerical errors in kinetic energy may have an effect on internal energy. One should pursue the reduction of the errors in kinetic energy by improving the discretization of the momentum equation. For example, the errors in the kinetic energy might be reduced by devising the advection term of momentum, as proposed by Morinishi et al. (1998).

Our method is, nevertheless, advantageous for the diagnosis of energy budget. If discretizations of all the energies are perfect, the conservation of the total energy is automatically assured. In reality, however, the errors are always associated with the discretizations of energies. If each energy is separately calculated, all the errors are accumulated to the total energy. For the energy budget of climate prediction, we cannot get more accurate estimations that this accumulated error of the total energy. Under the constraints of the total energy conservation, we can speculate upon what are the directions toward the next improvements.

The experiments in this study are preliminary and are intended only for the confirmation of the conservation of water and energy. If we perform a direct calculation of radiative–convective equilibrium by a long time integration, we may evaluate the quantitative impact of these improvements on the precipitation and the vapor content, in particular, and gain some insights into the credibility associated with climate simulations.

Acknowledgments. The author is grateful to F. Xiao, H. Tomita, and T. Nasuno for helpful discussions. He also appreciate the comments by two anonymous reviewers for improving the manuscript. The numerical calculations were done using the HITACH SR8000 at the University of Tokyo under the cooperative research efforts of the Center for Climate System Research, University of Tokyo, the NEC SX4 at the National Institute of Environmental Studies, the Compaq cluster system at the Frontier Research System for Global Change, and the parallel computers at the High-Tech Research Center of the Saitama Institute of Technology.

REFERENCES

Cullen, M. J. P., T. Davies, M. H. Mawson, J. A. James, S. C. Coutler, and A. Malcolm, 1997: An overview of numerical methods for the next generation U.K.NWP and climate model. *Numerical Methods in Atmospheric and Oceanic Modelling, The Andrew J. Robert Memorial Volume,* C. A. Lin et al., Eds., NRC Research Press, 425–444.

Emanuel, K., 1994: *Atmospheric Convection.* Oxford University Press, 580 pp.

Gallus, W., Jr., and M. Rančić, 1996: A non-hydrostatic version of the NMC's regional Eta model. *Quart. J. Roy. Meteor. Soc.,* **122,** 495–513.

Held, I. M., R. S. Hemler, and V. Ramaswamy, 1993: Radiative–convective equilibrium with explicit two-dimensional moist convection. *J. Atmos. Sci.,* **50,** 3909–3927.

Klemp, J. B., and R. B. Wilhemson, 1978: The simulation of three-dimensional convective storm dynamics. *J. Atmos. Sci.,* **35,** 1070–1096.

——, W. C. Skamarock, and J. Dudhia, cited 2000: Conservative split-explicit time integration methods for the compressible nonhydrostatic equations. [Available online at http://wrf-model.org/WG1/wg1_main.html.]

List, R. J., 1951: *Smithonian Meteorological Tables.* Smithonian Institution Press, 527 pp.

Morinishi, Y., T. S. Lund, O. V. Vasilyev, and P. Moin, 1998: Fully conservative higher order finite difference schemes for incompressible flow. *J. Comput. Phys.,* **143,** 90–124.

Nakajima, K., and T. Matsuno, 1988: Numerical experiments concerning the origin of cloud clusters in the tropical atmosphere. *J. Meteor. Soc. Japan,* **66,** 309–329.

Ooyama, K. V., 1990: A thermodynamic foundation for modeling the moist atmosphere. *J. Atmos. Sci.,* **47,** 2580–2593.

——, 2001: A dynamic and thermodynamic foundation for modeling the moist atmosphere with parameterized microphysics. *J. Atmos. Sci.,* **58,** 2073–2102.

Qian, J.-H., F. H. M. Semazzi, and J. S. Scroggs, 1998: A global nonhydrostatic semi-Lagrangian atmospheric model with orography. *Mon. Wea. Rev.,* **126,** 747–771.

Redelsperger, J.-L., and Coauthors, 2000: A GCSS model intercomparison for a tropical squall line observed during TOGA-COARE I: Cloud-resolving model. *Quart. J. Roy. Meteor. Soc.,* **126,** 823–863.

Satoh, M., 2002: Conservative scheme for the compressible nonhydrostatic models with the horizontally explicit and vertically implicit time integration scheme. *Mon. Wea. Rev.,* **130,** 1227–1245.

Semazzi, F. H. M., J. H. Qian, and J. S. Scroggs, 1995: A global nonhydrostatic semi-Lagrangian atmospheric model without orography. *Mon. Wea. Rev.,* **123,** 2534–2550.

Skamarock, W. C., and J. B. Klemp, 1992: The stability of time-split numerical methods for the hydrostatic and the nonhydrostatic elastic equations. *Mon. Wea. Rev.,* **120,** 2109–2127.

Smolarkiewicz, P. K., L. G. Margolin, and A. Wyszogrodzki, 2001: A class of nonhydrostatic global models. *J. Atmos. Sci.,* **58,** 349–364.

Tao, W.-K., J. Simpson, C.-H. Sui, C.-L. Shie, B. Zhou, K. M. Lau, and M. Moncrieff, 1999: Equilibrium states simulated by cloud-resolving models. *J. Atmos. Sci.,* **56,** 3128–3139.

Tomita, H., M. Tsugawa, M. Satoh, and K. Goto, 2001: Shallow water model on a modified icosahedral geodesic grid by using spring dynamics. *J. Comput. Phys.,* **174,** 579–613.

Tompkins, A. M., 2001: Organization of tropical convection in low vertical wind shears: The role of water vapor. *J. Atmos. Sci.,* **58,** 529–545.

——, and G. C. Craig, 1998: Radiative–convective equilibrium in a three-dimensional cloud ensemble model. *Quart. J. Roy. Meteor. Soc.,* **124,** 2073–2097.

——, and ——, 1999: Sensitivity of tropical convection to sea surface temperature in the absence of large-scale flow. *J. Climate,* **12,** 462–476.

Tsusima, Y., and S. Manabe, 2001: Influence of cloud feedback on annual variation of global mean surface temperature. *J. Geophys. Res.,* **106,** 22 635–22 646.

Xiao, F., and T. Yabe, 2001: Completely conservative and oscillationless semi-Lagrangian schemes for advection transportation. *J. Comput. Phys.,* **170,** 498–522.

——, T. Okazaki, and M. Satoh, 2003: An accurate semi-Lagrangian scheme for raindrop sedimentation. *Mon. Wea. Rev.,* **131,** 810–819.

Xu, K.-M., and D. A. Randall, 1999: A sensitivity study of radiative–convective equilibrium in the Tropics with a convective resolving model. *J. Atmos. Sci.,* **56,** 3385–3399.

Xue, M., K. K. Droegemeier, and V. Wong, 2000: The Advanced Regional Prediction System (ARPS)—A multi-scale nonhydrostatic atmospheric simulation and prediction model. Part I: Model dynamics and verification. *Meteor. Atmos. Phys.,* **75,** 161–193.

Yeh, K.-S., J. Cote, S. Gravel, A. Methot, A. Patoine, M. Roch, and A. Stainforth, 2002: The CMC–MRB Global Environmental Multiscale (GEM) model. Part III: Nonhydrostatic formulation. *Mon. Wea. Rev.,* **130,** 329–356.